# Space Mapping Optimization of Handset Antennas Exploiting Thin-Wire Models

Sheng Tu, *Student Member, IEEE*, Qingsha S. Cheng, *Senior Member, IEEE*, Yifan Zhang, *Student Member, IEEE*, John W. Bandler, *Life Fellow, IEEE*, and Natalia K. Nikolova, *Fellow, IEEE*

***Abstract*—A handset antenna modeling and design technique using space mapping (SM) is presented. Thin-wire models are exploited as coarse models in the SM algorithms, while the fine models are high-accuracy electromagnetic simulations. The thin-wire models capture the basic physics of handset antennas but are not as accurate as the fine model. On the other hand, they are computationally cheap when analyzed by the method of moments solvers. Detailed guidelines for building thin-wire models are provided. Two SM algorithms are employed: 1) implicit, input and output space mapping and 2) implicit and output space mapping. An internal dual-band patch antenna and an arm-folded planar inverted F antenna are designed through our approach. For comparison, direct optimizations have been performed in each example.**

***Index Terms*—Antenna design, electromagnetic (EM) optimization, handset antenna, method of moments (MoM), space mapping (SM).**

## I. Introduction

ELECTROMAGNETIC (EM) full-wave simulators have been widely employed in antenna design, performance estimation, and parametric analysis. The method of moments (MoM) [1] is one of the popular numerical methods and has been adopted by many commercial simulation software packages, such as FEKO [2], Sonnet's ***em*** [3], and IE3D [4]. The MoM simulations are reliable but at the cost of extensive CPU time, especially in complex design problems [5]–[7]. Handset antenna design using full-wave EM simulators is particularly challenging because of the high-performance requirements and limited space. Handset antennas are complicated structures often involving substrates. Sometimes, the chassis of the handset and other components (e.g., the battery and the voice speaker) are also included in the simulation. This can result in extremely lengthy EM simulations that prove to be prohibitive for the purpose of optimization.

Manuscript received October 20, 2012; revised January 16, 2013; accepted February 23, 2013. Date of publication March 26, 2013; date of current version July 01, 2013. This work was supported in part by the Natural Sciences and Engineering Research Council of Canada under Grants CRDPJ385785-09, STGP269670, RGPIN7239-11, and STPGP381153-09, and in part by Research In Motion Inc. and Bandler Corporation.

S. Tu, Y. Zhang, and N. K. Nikolova are with the Computational Electromagnetics Research Laboratory, Department of Electrical and Computer Engineering, McMaster University, Hamilton, ON L8S 4K1, Canada (e-mail: sheng.tu@hotmail.com; nikolova@ieee.org).

Q. S. Cheng and J. W. Bandler are with the Simulation Optimization Systems Research Laboratory, Department of Electrical and Computer Engineering, McMaster University, Hamilton, ON L8S 4K1, Canada.

Color versions of one or more of the figures in this paper are available online at http://ieeexplore.ieee.org.

Digital Object Identifier 10.1109/TAP.2013.2254695

Space mapping (SM) technology was first proposed for the design optimization of high-frequency structures [8]. It features a significant reduction of the computational cost. So far, SM algorithms have been successfully applied to the EM-based design of microwave devices, for example, filters, impedance-matching networks, multiplexers, antennas, etc. [7]–[15]. A principal task of SM is to establish a mapping between a fine model of the considered device and a suitable coarse/surrogate model. Usually, the fine model is accurate but CPU intensive. The coarse model is much faster but less accurate. The surrogate model is the mapped coarse model that matches the fine model better. Two desired aspects of a coarse model are: 1) low computational cost and 2) alignment capability with respect to the fine model. In the cases of SM-based optimization of microwave circuits (e.g., filters, impedance transformers, etc.), equivalent circuits, empirical and semi-analytical models, and their combinations have been shown as suitable coarse models [8]–[12].

In antenna design, a circuit-based coarse model is difficult to find due to the complexity of the structures. SM has been applied in antenna optimization using coarse-mesh EM coarse models [7]. There, the coarse and fine models use coarse- and fine-mesh simulations of the same structure, respectively. The same idea is then demonstrated in [13] for antenna-array optimization. In [14], this method has been further developed, where a kriging interpolation is performed based on the coarse-mesh simulations to generate a smooth coarse model. Another application of SM-based antenna optimization [15] uses library antenna models in existing databases, such as those in Antenna Magus [16]. There, the database coarse model is constructed based on a library antenna, which is, to some extent, geometrically similar to the fine-model structure.

Recently, wire models mimicking the geometry of complex handset antennas have been proposed by Geyi *et al.* [17]. The wire model is built by placing thin wires along the backbone or the outer edge of a handset antenna and the contour of the ground plane. Due to the edge effect, most of the current on the handset antenna is confined to its edges. The resulting wire model tends to retain a current distribution similar to that of the real solid antenna. Meanwhile, such wire models can be solved very quickly by the MoM.

The main problem with the wire models in [17] is that they may be prone to spurious resonances. Also, wire modeling has not been considered in the framework of optimization but only for preliminary estimation.

Here, we propose an approach to thin-wire modeling for handset antenna optimization using SM techniques. Guidelines for the thin-wire modeling are given taking into account the

antenna structure, its electrical size, as well as ground-plane effects (GPE). Compared with [17], our thin-wire model strategically adds extra thin wires to suppress spurious resonances while keeping the computational cost low. We integrate the proposed thin-wire modeling method with SM techniques to perform practical handset antenna design. Two examples [i.e., an internal dual-band patch antenna and an arm-folded planar inverted F antenna (PIFA)] are validated by our method using two SM algorithms: 1) implicit, input, and output SM (IIOSM), and 2) implicit and output SM (IOSM) [8], [9], [18]–[21].

## II. Space Mapping

### A. SM Basics

Generally, the design optimization problem is to solve

$$\boldsymbol{x}_f^* = \arg\min_{\boldsymbol{x}} U(\boldsymbol{R}_f(\boldsymbol{x})) \tag{1}$$

where $\boldsymbol{x}$ is the vector of $n$ design parameters, $\boldsymbol{x}_f^*$ is the optimal solution to be determined, and $\boldsymbol{R}_f \in \Re^{m\times 1}$ is the vector of $m$ responses of interest, for example, $|S_{11}|$ at $m$ sample frequency points. The subscript $f$ indicates the fine model and $U$ is a suitable objective function, for example, the minimax objective function with upper and lower specifications.

SM aims at establishing a mapping between the fine model and a coarse/surrogate model by matching their responses [8]. The time-expensive optimization solving (1) directly is avoided and replaced by the iterative optimization and update of the fast coarse/surrogate model. Therefore, a good estimate $\bar{\boldsymbol{x}}_f$ of $\boldsymbol{x}_f^*$ can be declared through the mapping [8]–[10].

In the surrogate-based SM [18]–[21], the coarse model is properly calibrated to become a so-called surrogate model after it is matched to the fine model. This requires the use of, for example, implicit [18], output [20], and/or input (original) SM [9]. Fig. 1 illustrates the various SM approaches. At the $i$th iteration, the general surrogate model can be defined as

$$\boldsymbol{R}_s^{(i)}(\boldsymbol{x}) = \boldsymbol{R}_c\left(\boldsymbol{B}^{(i)}\boldsymbol{x} + \boldsymbol{c}^{(i)}, \boldsymbol{p}^{(i)}\right) + \Delta\boldsymbol{R}^{(i)} \tag{2}$$

where, as shown in (3) at the bottom of the page, $K$ is a positive integer ($K = 2$ in our examples); $\boldsymbol{p} \in \Re^{q\times 1}$ is the vector of preassigned parameters (they are not elements of $\boldsymbol{x}$); $\Delta\boldsymbol{R} \in \Re^{m\times 1}$ is a response difference vector; and $\boldsymbol{B} \in \Re^{n\times n}$ and $\boldsymbol{c} \in \Re^{n\times 1}$ define linear mapping as suggested by Bandler *et al.* [8].

The implicit, output, and input SM build or enhance the mapping at different levels. The implicit SM aligns the surrogate and fine models by tuning the preassigned parameters $\boldsymbol{p}$ (see the yellow block in Fig. 1). The preassigned parameters can be, for example, the relative permittivity, the substrate thickness, etc. [18]. The initial values $\boldsymbol{p}^{(0)}$ are usually assigned to be the same as those in the fine model.

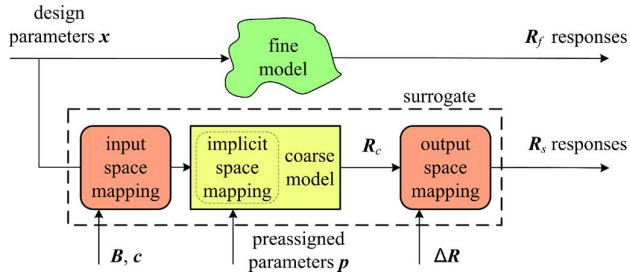


Fig. 1. Illustration of input, implicit, and output space mapping [7], [9].

The output SM (see Fig. 1) works directly at the response level using the vector $\Delta\boldsymbol{R}^{(i)}$. In our approach, see (3), $\Delta\boldsymbol{R}^{(i)}$ remains a zero vector during the iterations $i < K$. When $i \geq K$, the evaluation of $\Delta\boldsymbol{R}^{(i)}$ requires response information of the coarse and fine models in the last iteration. The implementation of output SM is avoided at the iterations $i < K$ because it would not help when there is significant misalignment between the fine model and surrogate model.

The input SM operates directly on the design parameters $\boldsymbol{x}$ by tuning $\boldsymbol{B}$ and/or $\boldsymbol{c}$ [see (2)]. The matrix $\boldsymbol{B}^{(0)}$ is initialized as the identity matrix and the vector $\boldsymbol{c}^{(0)}$ is initialized as a zero vector.

In general, the matrix $\boldsymbol{B}$, and the vectors $\boldsymbol{c}$ and $\boldsymbol{p}$ can be updated together at the $i$th iteration ($i > 0$) by solving

$$\left(\boldsymbol{B}^{(i)}, \boldsymbol{c}^{(i)}, \boldsymbol{p}^{(i)}\right) = \arg\min_{\boldsymbol{B},\boldsymbol{c},\boldsymbol{p}} \varepsilon^{(i)}(\boldsymbol{B}, \boldsymbol{c}, \boldsymbol{p}) \tag{4}$$

where $\varepsilon^{(i)}$ is the matching condition at the $i$th iteration that is calculated by

$$\varepsilon^{(i)}(\boldsymbol{B}, \boldsymbol{c}, \boldsymbol{p}) = \left\| \boldsymbol{R}_f\left(\boldsymbol{x}_f^{(i-1)}\right) - \boldsymbol{R}_c\left(\boldsymbol{B}\boldsymbol{x}_f^{(i-1)} + \boldsymbol{c}, \boldsymbol{p}\right) \right\|. \tag{5}$$

Here, $\|\|$ is a suitable norm. A sequence of points $\boldsymbol{x}_f^{(i)}$, $i = 0, 1, 2, \ldots$ is subsequently generated by solving

$$\boldsymbol{x}_f^{(i)} = \arg\min_{\boldsymbol{x}} U(\boldsymbol{R}_s^{(i)}(\boldsymbol{x})). \tag{6}$$

Equations (4) and (5) indicate the parameter extraction which is itself an optimization procedure using, for instance, a gradient-based optimizer; see, for example, [9]. The procedure can be executed efficiently because the evaluation of the surrogate model $\boldsymbol{R}_s^{(i)}(\boldsymbol{x})$ is usually fast. In some cases, for example, in [7], the matrix $\boldsymbol{B}$ is fixed as the identity matrix and/or $\boldsymbol{c}$ is fixed as $\boldsymbol{0}$. When the implicit SM is not applied, the vector $\boldsymbol{p}$ is fixed at its initial values.

The termination criteria of SM are: a) convergence is achieved (e.g., the change in objective function value is small); b) the design specification is satisfied; and c) the maximum iteration number is reached [7]–[10], [14].

$$\Delta\boldsymbol{R}^{(i)} = \begin{cases} \boldsymbol{R}_f\left(\boldsymbol{x}_f^{(i-1)}\right) - \boldsymbol{R}_c\left(\boldsymbol{B}^{(i-1)}\boldsymbol{x}_f^{(i-1)} + \boldsymbol{c}^{(i-1)}, \boldsymbol{p}^{(i-1)}\right), & i \geq K \\ 0 & 0 \leq i < K. \end{cases} \tag{3}$$

### B. Our SM Algorithm

In this paper, a surrogate model based on a combination of implicit, output, and/or input SM is employed. Our SM optimization algorithm performs the following steps:

Step 1) Create a suitable thin-wire model and choose the preassigned parameter vector $\boldsymbol{p}$. Set $i = 0$ and initialize $\boldsymbol{B}^{(i)} = \boldsymbol{1}$, $\boldsymbol{c}^{(i)} = \boldsymbol{0}$, $\Delta\boldsymbol{R}^{(i)} = \boldsymbol{0}$, and $\boldsymbol{p}^{(i)}$ to obtain the initial surrogate model based on (2) and (3).

Step 2) Solve (6) to obtain $\boldsymbol{x}_f^{(i)}$.

Step 3) Evaluate the fine model to obtain $\boldsymbol{R}_f(\boldsymbol{x}_f^{(i)})$.

Step 4) Stop if the termination criterion (a), (b), and/or (c) is satisfied.

Step 5) Update $\boldsymbol{B}^{(i+1)}$, $\boldsymbol{c}^{(i+1)}$, $\boldsymbol{p}^{(i+1)}$ through parameter extraction using (4) and (5).

Step 6) Update the surrogate model to $\boldsymbol{R}_s^{(i+1)}(\boldsymbol{x})$ using (2) and (3).

Step 7) Set $i = i+1$, and go to Step 2).

Note that the fine model is only evaluated once in each SM iteration [see Step 3)] while there may be multiple calls to the coarse model during the parameter extraction process [see Step 5)]. The computational cost of Step 5) is kept at an acceptable level due to the low cost of the surrogate model. The number of iterations of the space mapping algorithm is usually quite small. In contrast, in conventional direct optimization, multiple fine model evaluations may be required in each iteration, and the total number of iterations is much higher.

## III. Thin-Wire Modeling Methodology

The basic idea of thin-wire modeling is to use as few thin wires as possible to represent the solid metallic parts of the antenna structure. The substrate material of the antenna structure can be completely removed in the thin-wire model. Alternatively, the thin-wire model can be immersed in an infinite homogeneous material. The property parameters of the infinite homogeneous material, for example, are the permittivity and the loss tangent, can be considered as preassigned parameters for the implicit SM formulation. We will now list the guidelines for the model construction.

### A. Antenna Thin-Wire Modeling

In this subsection, we consider the main antenna structure excluding the ground plane. There are three rules when representing the handset antenna geometry. (A1) Place the wires along the shape edges, for example, the contours or the outer edges of the strips and/or the patches. Often, a single wire can replace a strip segment of the antenna. (A2) At places where current is injected or current density lines converge or diverge, additional wires should be placed along the current density lines. Such places are the connections to the feed line or to the shorting pin/strip or to the neighboring wires. (A3) Inspecting the mesh of the handset antenna created by the fine EM simulator allows us to identify places where additional wires may be needed. Such places are usually the areas with very fine MoM mesh.

Rules (A1) and (A2) address the basic thin-wire model, while rule (A3) is used to improve the model and to eliminate spurious resonances.

### B. Ground Plane Thin-Wire Modeling

The ground plane of a handset antenna often has a size of about 60 $\times$ 100 mm. The ground-plane size and shape significantly impact the antenna's performance if the size is below a wavelength [22]. For example, a square ground plane with an edge length smaller than $\lambda/5$, where $\lambda$ is the wavelength, would strongly affect the antenna resonant frequency [22].

In the higher frequency ranges in the wireless communication bands: GSM1800/1900, PCS1900, WLAN 2.4, etc., the ground-plane size is comparable to the wavelength. In this case, the GPE is usually weak and can be neglected. Hence, the finite ground plane can be simply replaced by an infinite ground plane in the thin-wire model. In the MoM, the addition of an infinite ground plane does not have an impact on the computational time due to the use of a suitable Green's function.

On the other hand, the GPE is usually strong in the lower frequency ranges such as GSM800/900, PCS900, etc. In this case, the following rules are helpful. (G1) Place wires in a loop along the contour of the ground plane. (G2) At places where current is injected or current density lines converge or diverge (e.g., the feeding/shorting point), wires need to be placed and connected with the contour loop. (G3) To suppress the spurious resonances, extra wires are added to increase the grid density of the thin-wire ground structure. As a rule of thumb, it is suggested that the grid size not be bigger than $(\lambda/10)^2$.

Rules (G1) and (G2) provide a basic thin-wire ground structure whose wire segments are likely comparable to the wavelength $\lambda$. This is likely to lead to spurious resonances and, consequently, rule (G3) needs to be applied.

In addition, if it is not subject to optimization, the ground plane thin-wire structure should be fixed (i.e., no geometrical changes are made during the entire optimization process).

### C. Wire Mesh Setting and Computational Cost Reduction

The MoM solver discretizes the computer-aided design (CAD) model into a set of computational cells [1]. The thin-wire model employs the general rules of MoM wire segmentation. On the other hand, a coarse mesh could be adequate for the ground plane of the thin-wire model. Note that it is recommended that the mesh settings (e.g., the maximum segment size in [2]) be fixed throughout the optimization. The radius of the line segment of the thin-wire model is set to a uniform value far smaller than $\lambda$ (e.g., $\lambda/10^3$).

Due to the significantly reduced number of unknowns, the wire model achieves drastic reduction of the computational cost.

## IV. Examples

Two validation examples are presented in this section where the MoM-based simulator [2] is used. The SM algorithms—IIOSM and IOSM—are implemented in MATLAB [23]. In each example, the fine model is the finely meshed simulation model of a handset antenna. The coarse model is the thin-wire model created by our approach. Direct optimization (DO) procedures using the FEKO optimizer *Simplex Nelder-Mead method* and the MATLAB optimizer *Sequential Quadratic Programming* are, respectively, performed in both examples for comparison. The starting point of the DO is the same as that of the SM approach. The optimization convergence accuracy

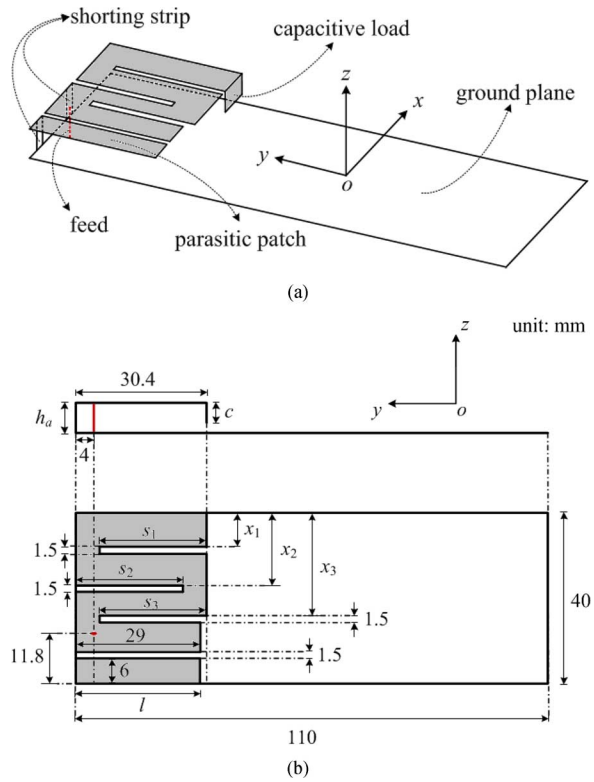


Fig. 2. Geometry of the internal dual-band patch antenna with dimensions in millimeters. (a) 3-D view, and (b) side and top views.

of the FEKO optimizer is set by default [24]. In MATLAB, the *fminimax* function is adopted [25].

### A. Internal Dual-Band Patch Antenna

We consider an internal dual-band patch antenna for handsets covering the bands E-GSM900 (0.88 GHz–0.96 GHz), GSM1800 (1.71 GHz–1.88 GHz), DECT (1.88 GHz–1.90 GHz), PCS1900 (1.85 GHz–1.99 GHz), and universal mobile telephone services (UMTS) (1.90 GHz–2.17 GHz) [26]. The antenna structure is shown in Fig. 2. The shorted meander-line patch with the capacitive load at the end is the main element of the antenna contributing to the dual-band resonances. A shorted parasitic patch is added on the side to widen the bandwidth in the lower frequency band (i.e., E-GSM900 [27]). Eight variables are tuned in the design (i.e., $\boldsymbol{x} = [x_1\ x_2\ x_3\ s_1\ s_2\ s_3\ c\ l]^T$). As shown in Fig. 2, these are the locations and the lengths of the slots on the main element, the length of the capacitive plate, and the length of the parasitic patch. The radius of the feeding pin is 0.5 mm, the width of the shorting strip is 2 mm, and the antenna height is $h_a = 7$ mm. All of the other dimensions are given in Fig. 2(b).

The design specifications are

$$|S_{11}| \le 0.5 \text{ for } 0.88 \text{ GHz} \le \omega \le 0.96 \text{ GHz},$$
$$|S_{11}| \le 0.5 \text{ for } 1.71 \text{ GHz} \le \omega \le 2.17 \text{ GHz}.$$

Here, the problem is cast into a minimax optimization problem, namely

$$\min_{\boldsymbol{x}} \{U(\boldsymbol{x})\} \tag{7}$$

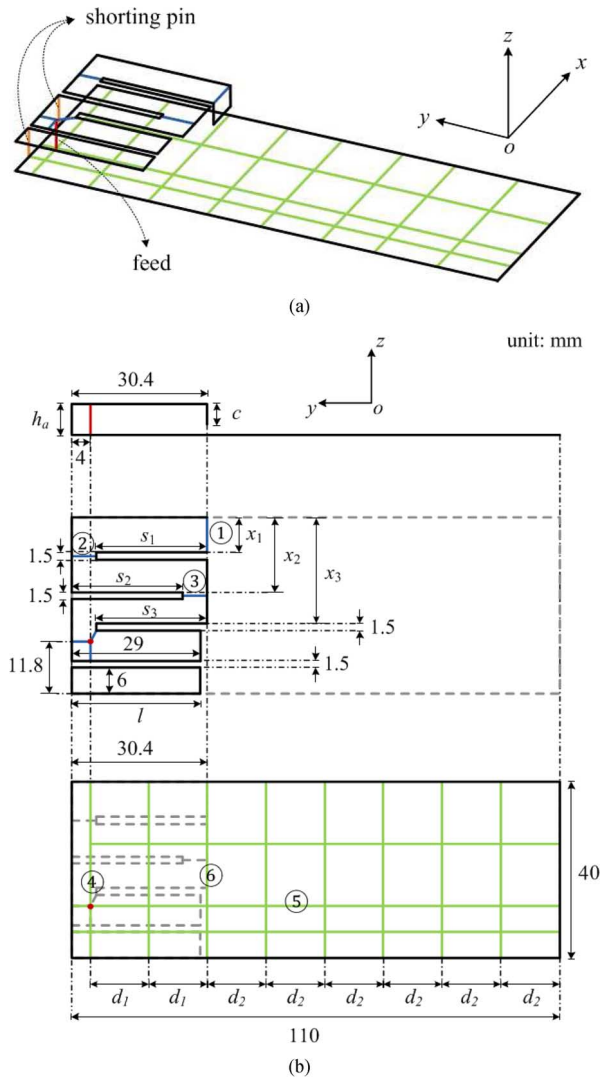


Fig. 3. Geometry of the thin-wire coarse model of the internal dual-band patch antenna. (a) 3-D view, and (b) side view, antenna top view and ground plane top view.

and

$$U(\boldsymbol{x}) = \max_{1 \le j \le N} \left\{ \left| S_{11}^{(j)}(\boldsymbol{x}) \right| - \bar{S}_{11} \right\} \tag{8}$$

where $|S_{11}^{(j)}(\boldsymbol{x})|$ is the linear magnitude of the $S$-parameter response at the $j$th frequency sample point and $U(\boldsymbol{x})$ is the objective function. There are 5 and 13 sample frequency points in the upper and lower frequency bands, respectively. The total number of sample frequencies is $N = 18$, and the specification is $\bar{S}_{11} = 0.5$.

The corresponding thin-wire coarse model is shown in Fig. 3. The thin-wire modeling for the antenna part follows rules (A1)–(A3) in Section III-A; see the antenna top view in Fig. 3(b). The orange lines in Fig. 3(a) represent the shorting strips of the fine model shown in Fig. 2. Since the width of each shorting strip is fixed at 2 mm, a single wire is used to replace it. The blue lines in Fig. 3 are the additional wires. The gaps between the tip of the feeding pin and the neighboring wires are bridged by the three blue wires as shown in the antenna top

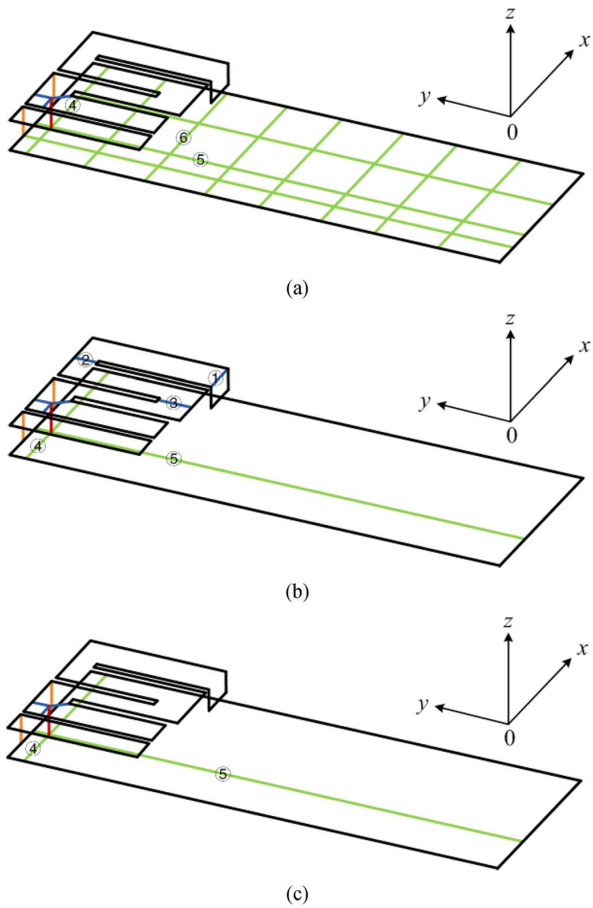


Fig. 4. Geometries of three thin-wire test models of the internal dual-band patch antenna. (a) Test model I, (b) test model II, and (c) test model III.

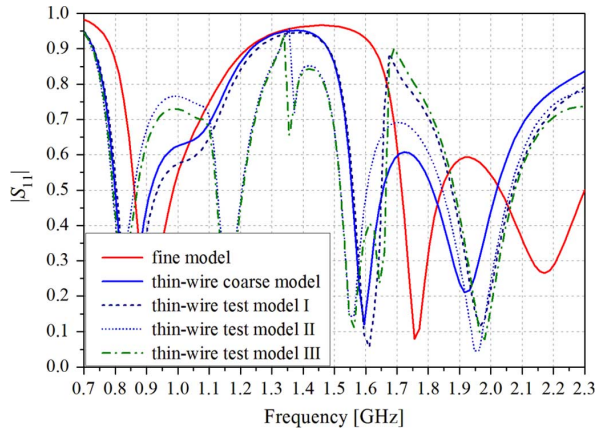


Fig. 5. $|S_{11}|$ responses of the thin-wire coarse model and the thin-wire test models at the initial points $\boldsymbol{x}_f^{(0)}$ and $\boldsymbol{p}^{(0)}$ for the internal dual-band patch antenna. $\boldsymbol{x}_f^{(0)}$ is obtained by directly optimizing the coarse thin-wire model at the initial step.

view of Fig. 3(b). The blue wire ① is added to represent the edge connecting the capacitive load. The blue wires ② and ③ are added between the closely spaced parallel edges of the solid metallic strip.

Given the significant GPE in the lower frequency band, the modeling of the finite ground plane follows rules (G1)–(G3) in Section III-B. As shown in Fig. 3(b), the resulting thin-wire ground plane is mesh like. Beside the wires along the contour of the original ground plane, extra wires are added (i.e., the green lines shown in Fig. 3). The green wires ④ and ⑤ are added at the connection with the feeding pin, while the green wire ⑥ is added right underneath the wires representing the capacitive load. The other green wires are added to increase the grid density as suggested in Section III-B. They are placed at equal distances of $d_1 = 15.2$ mm and $d_2 \approx 13.27$ mm as shown in Fig. 3(b).

To demonstrate the effect of the additional wires, the three thin-wire test models are created by removing certain wires from the coarse model in Fig. 3. As shown in Fig. 4, the thin-wire test models have the following wires removed: (I) the blue wires ①, ②, and ③; (II) the green wire ⑥ and other unmarked green wires; and (III) all wires described in (I) and (II). Fig. 5 shows the $S$-parameter responses of the fine model, the thin-wire coarse model, as well as the thin-wire test models I, II, and III, at the point $\boldsymbol{x}_f^{(0)} = [8.12\ \ 17.92\ \ 24.81\ \ 23.00\ \ 24.50\ \ 25.19\ \ 4.05\ \ 28.40]^T$ mm. $\boldsymbol{x}_f^{(0)}$ is obtained by directly optimizing the thin-wire coarse model in Fig. 3. The antenna height of all the thin-wire test models ($h_a = 7$ mm) and the relative permittivity of free space ($\varepsilon_r = 1$) are the same as in the fine model.

It can be seen in Fig. 5 that in the frequency range from 0.7 to 2.3 GHz, the fine model has three main resonances around 0.92 GHz, 1.75 GHz, and 2.16 GHz. The thin-wire coarse model also has three main resonances which are around 0.85 GHz, 1.6 GHz, and 1.92 GHz. The thin-wire test model I has similar behavior as the thin-wire coarse model but it is misaligned significantly with the fine model over the frequencies from 1.6 to 1.9 GHz. The thin-wire test model II has two obvious spurious resonances around 1.15 and 1.35 GHz. The response of the thin-wire test model III appears like the averaged responses of the thin-wire models I and II but has one more spurious resonance at around 1.65 GHz. This demonstrates that the additional blue wires ①, ②, and ③ mainly affect the higher frequency responses, while the green wire ⑥ and the other unmarked green wires affect the lower frequency responses. The additional wires are able to eliminate the spurious resonances and improve the alignment between the thin-wire coarse model and the fine model.

It also can be observed that the response of the thin-wire coarse model is shifted in frequency compared to the fine model. The shift is more significant at higher frequencies (above 1.4 GHz) compared with the shift at lower frequencies (below 1 GHz). The frequency shift can be overcome by calibrating the preassigned parameters of the thin-wire coarse model using implicit SM. To compensate for the different amounts of shift in the two working bands, a separate preassigned parameter vector is considered for each band. Here, the preassigned parameters of the thin-wire coarse model are set to the relative permittivity $\varepsilon_r$ and the antenna height $h_a$. The preassigned parameter vector at the $i$th iteration of SM is denoted as $\boldsymbol{p}_\xi^{(i)} = [\varepsilon_{r,\xi}^{(i)}\ \ h_{a,\xi}^{(i)}]^T$, where $\xi = 1, 2$ corresponds to the lower and upper frequency bands, respectively. In the beginning, $\boldsymbol{p}_\xi^{(0)} = [1\ \ 7\ \text{mm}]^T$ $(\xi = 1, 2)$ is the same as that in the fine model.

Table I gives the mesh setting and time cost of a single-response simulation of the fine model and its thin-wire coarse model. Note that the thin-wire coarse model adopts fine and coarse meshing for the antenna and the ground plane, respectively. The wires of the ground plane are coarsely meshed with

TABLE I
COMPARISON OF THE COMPUTATIONAL COSTS OF THE COARSE AND FINE MODELS IN THE INTERNAL DUAL-BAND PATCH ANTENNA EXAMPLE

| Model type | Technique | Meshing method | Mesh cell number | Frequency sweep time |
|---|---|---|---|---|
| Coarse model | Thin-wire model | Fine mesh (antenna) + coarse mesh (ground plane) | 165 line segments | 17 seconds |
| Fine model | Original CAD model | Fine mesh | 1428 triangles & 2 line segments | 9 minutes and 40 seconds |

*Number of mesh cells and frequency sweep time of each model are measured at the initial points $\boldsymbol{x}_f^{(0)}$ and $\boldsymbol{p}^{(0)}$ with 81 frequency sample points from 0.7 GHz to 2.3 GHz.

the segment size of $\lambda_0/5$, where $\lambda_0$ is the free space wavelength at 2.3 GHz. The wires of the antenna part use a segment size of $\lambda_0/20$.

Fig. 6 shows the current distributions of the fine model and the corresponding thin-wire coarse model at the central frequency of each band. The two distributions are similar.

Next, the results from the design optimization are presented. Fig. 7 shows the objective function value of the SM optimization process versus the iteration number. The IIOSM algorithm achieved its best solution at the 4th iteration, while the IOSM algorithm achieved its best solution at the 6th iteration. Table II summarizes the computational cost of each SM approach to obtain its best solution. Fig. 8 shows the initial and best-solution responses of the fine and the surrogate models. Initially, the fine and surrogate models exhibit poor responses. However, their responses at the best solution found by each SM algorithm satisfy the design specifications and are aligned very well.

The DO results are also summarized in Table II. Compared with the DO methods, our SM approaches solve this antenna design problem significantly better in CPU time and solution reached.

### B. Arm-Folded PIFA

This antenna is printed on the surface of the box-shaped component shown in Fig. 9. The walls of the component are made of FR4 substrate that has a relative dielectric constant of 4.4, a dielectric loss tangent of 0.002, and a thickness of 0.8 mm. Air is assumed inside the component. The height of the component is $h_b = 5$ mm. Only the ground plane (the light gray area on the bottom side of the component) and the antenna (the dark gray area) are metallic. The arm-folded PIFA is formed by the metal strips with a uniform width of 1 mm. The antenna is located at one corner of the box-shaped component with an equally folded arm to reduce its size. This antenna is designed for the WLAN 2.4 GHz band (2.412 GHz–2.484 GHz). The design specification is

$$|S_{11}| \leq 0.3162 \text{ for } 2.4 \text{ GHz } \leq \omega \leq 2.5 \text{ GHz}.$$

The design problem is to solve the minimax optimization problem stated in (7) and (8) with six frequency sample points in the band from 2.4 to 2.5 GHz, and the specification is $\bar{S}_{11} = 0.3162$.

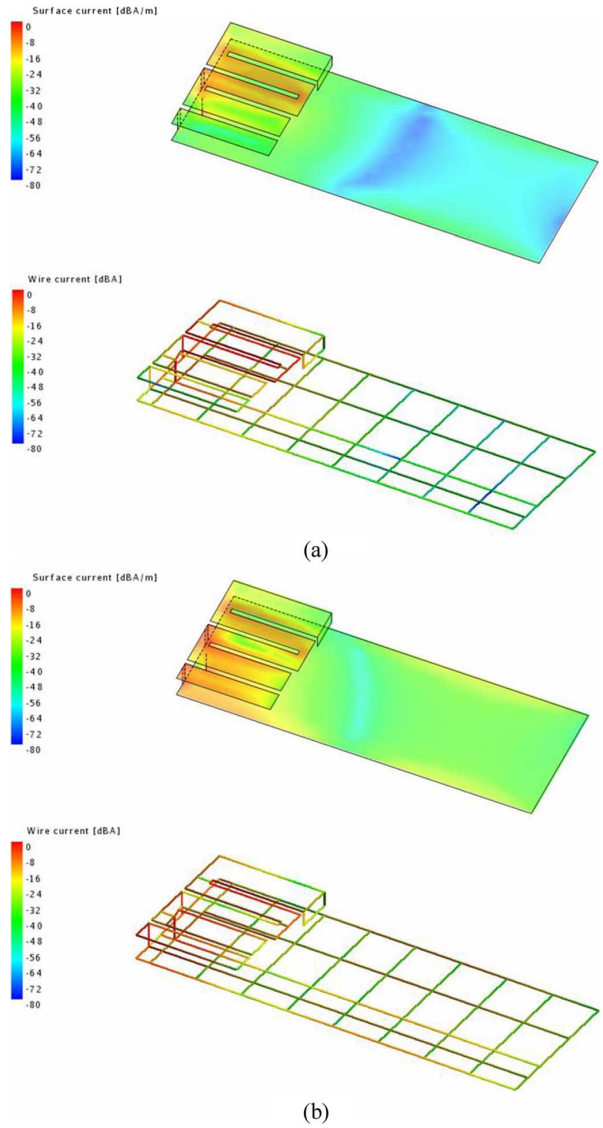


Fig. 6. Current distributions of the fine model and the thin-wire coarse model at the central frequency of each band: (a) 0.92 GHz and (b) 1.94 GHz at the initial points $\boldsymbol{x}_f^{(0)}$ and $\boldsymbol{p}^{(0)}$ for the internal dual-band patch antenna.

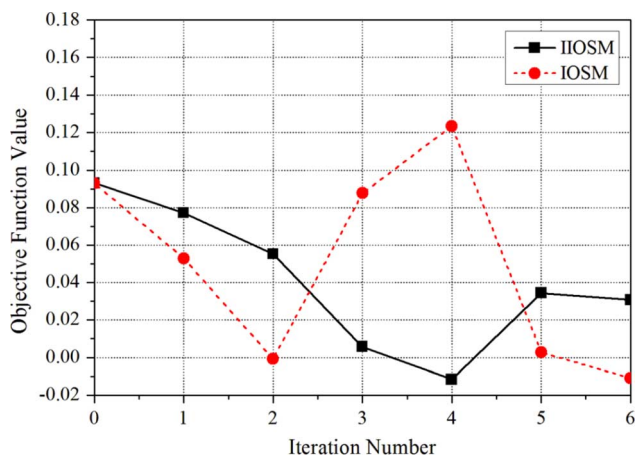


Fig. 7. Objective function value versus the iteration number using IIOSM or IOSM for the internal dual-band patch antenna.

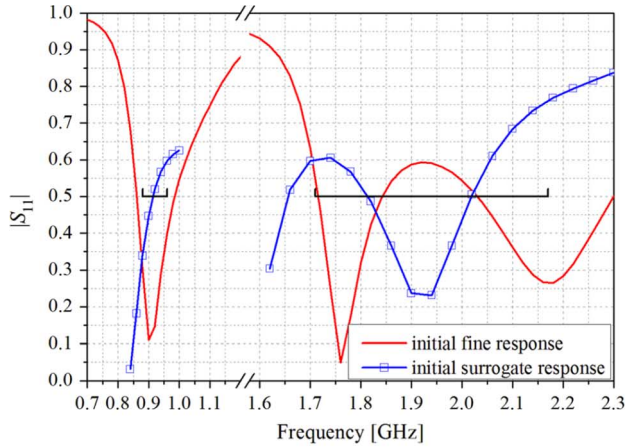


(a)

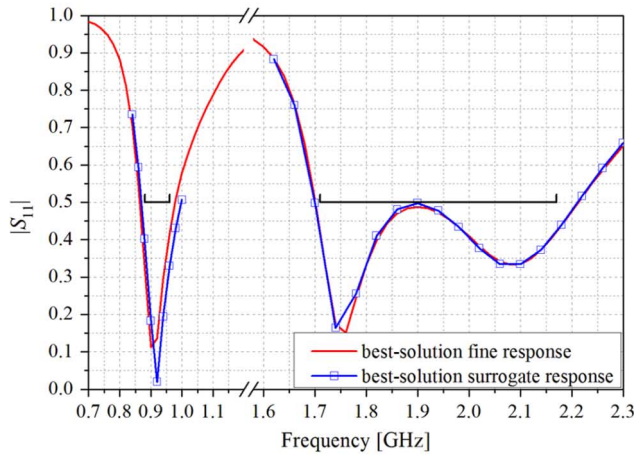


(b)

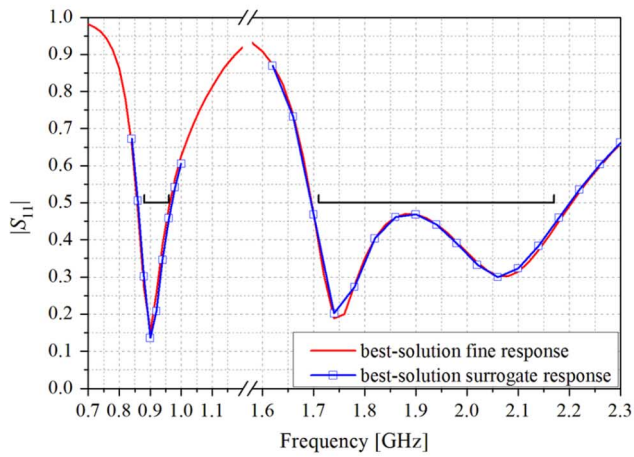


(c)

Fig. 8. Internal dual-band patch antenna optimization results. (a) Initial fine and surrogate $|S_{11}|$ responses at the initial points $\boldsymbol{x}_f^{(0)}$ and $\boldsymbol{p}^{(0)}$. Fine and surrogate best-solution $|S_{11}|$ responses obtained at: (b) the 4th iteration of IIOSM and (c) the 6th iteration of IOSM.

TABLE II
COMPARISON OF THE COMPUTATIONAL COSTS OF THE PROPOSED APPROACH AND DIRECT OPTIMIZATION (DO) IN THE INTERNAL DUAL-BAND PATCH ANTENNA EXAMPLE

| | | IIOSM (4th iteration) | IOSM (6th iteration) | DO (Matlab) | DO (FEKO) |
|---|---|---|---|---|---|
| Optimal solution (mm) | $x_1$ | 8.40 | 9.76 | 9.22 | 9.97 |
| | $x_2$ | 16.37 | 15.29 | 15.81 | 17.06 |
| | $x_3$ | 22.79 | 22.07 | 24.89 | 25.53 |
| | $s_1$ | 24.01 | 23.51 | 25.35 | 23.06 |
| | $s_2$ | 23.33 | 23.07 | 27.45 | 23.96 |
| | $s_3$ | 25.61 | 23.11 | 25.53 | 25.21 |
| | $c$ | 5.45 | 5.94 | 4.00 | 4.33 |
| | $l$ | 28.94 | 29.03 | 29.63 | 28.62 |
| Fine model evaluation number | | 5 | 7 | 1067 | 244 |
| Total time (hour) | | 18.73 | 19.65 | 61.05 | 43.35 |
| Objective function value | | -0.0116 | -0.0110 | 0.0279 | 0.0705 |

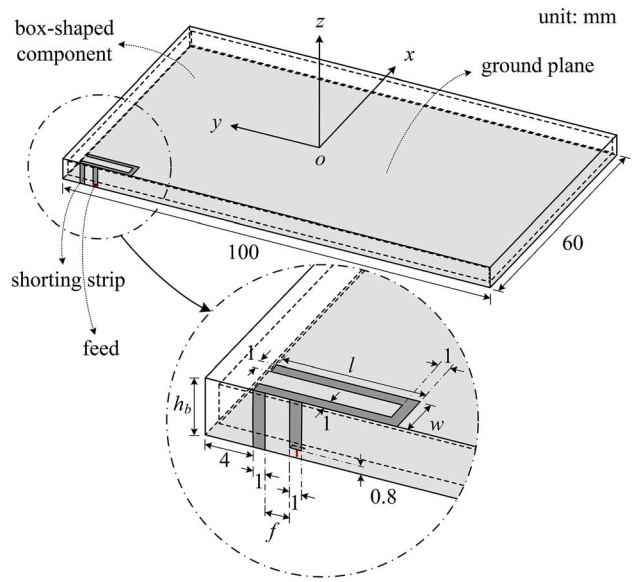


Fig. 9. Geometry of the arm-folded PIFA with dimensions in millimeters.

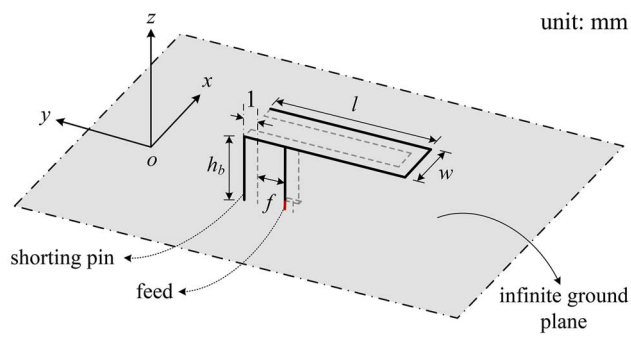


Fig. 10. Geometry of the thin-wired coarse model of the arm-folded PIFA.

The thin-wire coarse model is shown in Fig. 10. It consists of a single wire representing each strip and an infinite ground plane in the air. Since the antenna structure is simple and the GPE is not strong over the frequency band of interests, the thin-wire modeling of the antenna part adopts rule (A1) in Section III-A and the infinite ground-plane approximation (see Section III-B). As shown in Fig. 9, the design parameters are $\boldsymbol{x} = [l \ w \ f]^T$. The preassigned parameters are $\boldsymbol{p} = [\varepsilon_r \ h_b]^T$ (i.e., the free-space relative permittivity and the antenna height). Initially, $\boldsymbol{p}^{(0)} = [1 \ 5 \ \text{mm}]^T$ is the same as that of the fine model.

Table III gives the mesh setting and the simulation time of the fine and coarse models, respectively, for one frequency sweep. In the fine simulation model, most of the computational cells are generated for the box-shaped component. In contrast, the

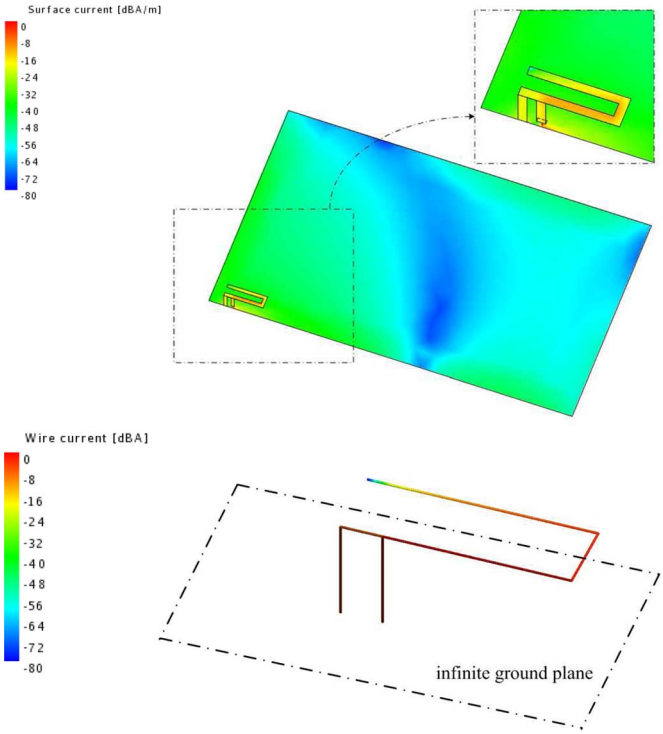


Fig. 11. Current distributions of the fine model and the thin-wire coarse model at the central frequency of 2.45 GHz at the initial points $\boldsymbol{x}_f^{(0)}$ and $\boldsymbol{p}^{(0)}$ for the arm-folded PIFA. $\boldsymbol{x}_f^{(0)}$ is obtained by directly optimizing the coarse thin-wire model at the initial step.

TABLE III
COMPARISON OF COMPUTATIONAL COSTS OF THE COARSE AND FINE MODELS IN THE ARM-FOLDED PIFA EXAMPLE

| Model type | Technique | Meshing method | Mesh cell number | Frequency sweep time |
|---|---|---|---|---|
| Coarse model | Thin-wire model | Fine mesh (antenna) + special Green's function (ground plane) | 35 line segments | 3 seconds |
| Fine model | Original CAD model | Fine mesh | 3307 triangles & 5 line segments | 35 minutes 57 seconds |

*Number of mesh cells and frequency sweep time of each model are measured at the initial points $\boldsymbol{x}_f^{(0)}$ and $\boldsymbol{p}^{(0)}$ with 10 frequency sample points from 2.36 GHz to 2.54 GHz.

thin-wire coarse model is computationally much cheaper because it only contains metallic wires and an infinite ground plane without substrate. The similar current distributions of the fine and the thin-wire coarse models can be observed at 2.45 GHz in Fig. 11.

The objective function value of the SM optimization process versus the iteration number is presented in Fig. 12. The IIOSM algorithm found its best solution at the 6th iteration, while the IOSM found its best solution at the second iteration. Table IV summarizes the computational cost of each SM algorithm to obtain its best solution. The initial and best-solution responses of the fine and surrogate models are shown in Fig. 13. Initially, neither the fine model nor the surrogate model responses satisfy the design specification [Fig. 13(a)]. At the initial point $\boldsymbol{x}_f^{(0)}$, the SM approach aligns the surrogate-model response $\boldsymbol{R}_s(\boldsymbol{x}_f^{(0)})$

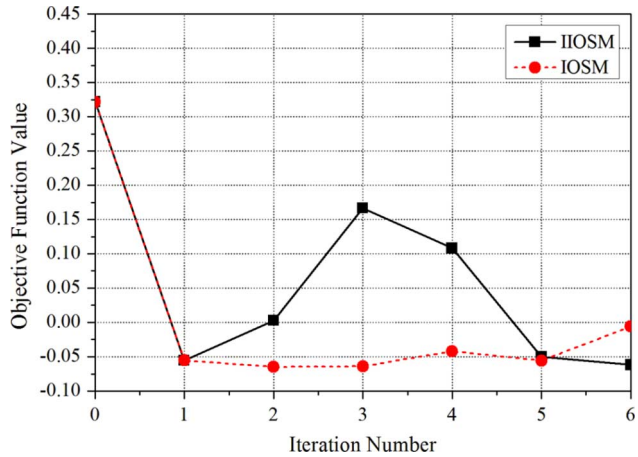


Fig. 12. Objective function value versus the iteration number using IIOSM or IOSM for the arm-folded PIFA.

with the fine-model response $\boldsymbol{R}_f(\boldsymbol{x}_f^{(0)})$ by tuning $\boldsymbol{p}$ and $\boldsymbol{c}$; see (2). The updated surrogate model is optimized to obtain $\boldsymbol{x}_f^{(1)}$. These tuning and optimizing procedures are repeated until one of the termination criteria is satisfied. Good alignment and an optimal solution can be acquired within several iterations of SM, as shown in Fig. 13(b) and (c).

The MATLAB and FEKO optimizers have been applied for DO of the same structure with the same initial design parameter. The results are also presented in Table IV for comparison. Compared with the DO methods, both SM schemes can solve the problem much more efficiently. Also note that a good solution is already obtained at the first iteration of each SM optimization (see Fig. 12). This can be useful for time-sensitive design tasks.

## V. DISCUSSION

An important observation in this study is that the thin-wire model tends to shift the $|S_{11}|$ response of the handset antenna in the frequency domain [see Figs. 5, 8(a) and 13(a)]. Also, the optimal solution of the surrogate model may not satisfy the design specification at the initial step. This is an indication that the misalignment between the fine model and its corresponding thin-wire coarse model is significant. Such problems are overcome mainly by the implementation of implicit SM.

In both validation examples, it can be seen that the objective function value fluctuates over the iteration numbers (see Figs. 7 and 12). To improve algorithm convergence, the trust-region-based SM technique [28], [29] can be considered at the cost of computational overhead. But we obtained good results without it.

The proposed approach mainly applies to the geometry of the metal parts of a handset antenna. If the fine model includes other metal components (e.g., the battery), then the corresponding thin-wire structure must be included following the guidelines in Section III. When inhomogeneous materials or high-contrast materials (e.g., ceramic or ferromagnetic components) are included in the fine model, omitting these components may result in insurmountable misalignment between the fine and surrogate models. In this case, the thin-wire coarse models reach their limit, and other coarse-model types that could address the material properties are required.

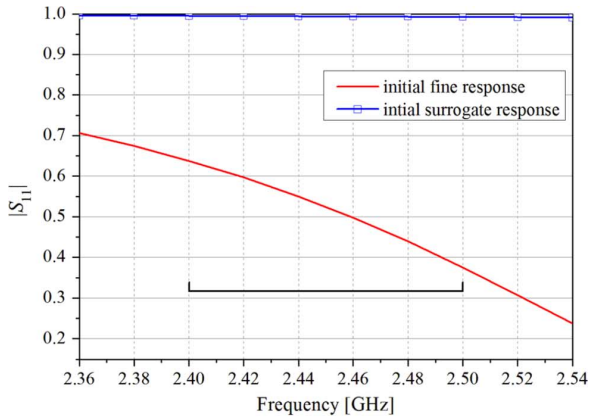


(a)

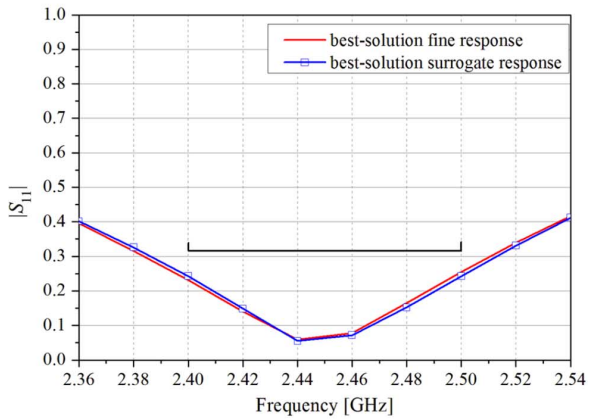


(b)

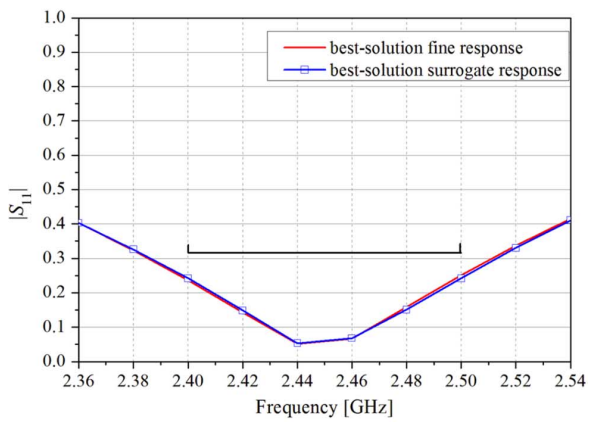


(c)

Fig. 13. Arm-folded PIFA optimization results. (a) Initial fine and surrogate $|S_{11}|$ responses at the initial points $\boldsymbol{x}_f^{(0)}$ and $\boldsymbol{p}^{(0)}$. The fine and surrogate best-solution $|S_{11}|$ responses obtained at: (b) the 6th iteration of IIOSM, and (c) the second iteration of IIOSM.

Since the proposed thin-wire model captures the physical characteristic (current distribution) of the fine model, in principle, the radiation pattern can be also optimized by our approach. The radiation patterns, however, are rarely an optimization objective in the design of handset antennas because these antennas are relatively small and feature fairly isotropic radiation. Additional tests have also been performed to study the radiation efficiencies of the coarse and fine models of each example in Section IV. In both cases, similar responses are observed between the fine and the thin-wire coarse models. Thus, we expect that the proposed technique would work if the optimization objective includes radiation efficiency. On the other hand, if the loss of power is mainly caused by lossy substrate materials or other nonmetal components, our thin-wire model may not provide a good coarse model for radiation-efficiency optimization.

TABLE IV
COMPARISON OF COMPUTATIONAL COSTS OF THE PROPOSED APPROACH AND DIRECT OPTIMIZATION (DO) IN THE ARM-FOLDED PIFA EXAMPLE

| | | IIOSM (6th iteration) | IOSM (2nd iteration) | DO (Matlab) | DO (FEKO) |
|---|---|---|---|---|---|
| Optimal solution (mm) | $l$ | 10.58 | 10.51 | 11.29 | 11.46 |
| | $w$ | 4.48 | 4.49 | 3.84 | 3.50 |
| | $f$ | 0.56 | 0.50 | 0.82 | 1.58 |
| Fine model evaluation number | | 7 | 3 | 86 | 46 |
| Total time (hour) | | 10.61 | 3.39 | 47.61 | 27.38 |
| Objective function value | | -0.0619 | -0.0650 | -0.0525 | -0.0435 |

## VI. CONCLUSION

A space-mapping-based modeling and design technique is proposed for handset antennas. This approach exploits fast thin-wire coarse models solved by the MoM. The guidelines for constructing a suitable thin-wire coarse model are given in detail. Our proposed SM schemes take full advantage of the thin-wire coarse models. The efficiency of our approach is demonstrated through two validation examples, where an internal dual-band patch antenna and an arm-folded PIFA are optimized. The results confirm that fast and accurate designs can be achieved by the proposed approach. The time savings compared to direct EM-based optimization are significant.

## ACKNOWLEDGMENT

The authors would like to thank Dr. M. H. Bakr and M. Ghassemi of McMaster University for their insightful comments and useful ongoing discussions.

## REFERENCES

[1] R. F. Harrington, *Field Computation by Moment Method*. New York: IEEE, 1993.
[2] FEKO, suite 6.0, EM Software & Systems, Inc. USA, 2010. [Online]. Available: http://www.feko.info/download
[3] Sonnet's *em*, suite 12.52. Sonnet Software, Inc., North Syracuse, NY, USA, 2009.
[4] IE3D. ver. 14, Zeland Software, Inc., CA, 2008.
[5] Y. Zhang, N. K. Nikolova, and M. H. Bakr, "Input impedance sensitivity analysis of patch antenna with discrete perturbations on method-of-moment grids," *Appl. Comput. Electromagn. Soc. J.*, vol. 25, no. 10, pp. 867–876, Oct. 2010.
[6] Y. Zhang, N. K. Nikolova, and M. K. Meshram, "Design optimization of planar structures using self-adjoint sensitivity analysis," *IEEE Trans. Antennas Propag.*, vol. 60, no. 6, pp. 3060–3066, Jun. 2012.
[7] J. Zhu, J. W. Bandler, N. K. Nikolova, and S. Koziel, "Antenna optimization through space mapping," *IEEE Trans. Antennas Propag.*, vol. 55, no. 3, pp. 651–657, Mar. 2007.
[8] J. W. Bandler, R. M. Biernacki, S. H. Chen, P. A. Grobelny, and R. H. Hemmers, "Space mapping technique for electromagnetic optimization," *IEEE Trans. Microw. Theory Tech.*, vol. 42, no. 12, pp. 2536–2544, Dec. 1994.
[9] J. W. Bandler, Q. S. Cheng, S. A. Dakroury, A. S. Mohamed, M. H. Bakr, K. Madsen, and J. Sondergaard, "Space mapping: The state of the art," *IEEE Trans. Microw. Theory Tech.*, vol. 52, no. 1, pp. 337–361, Jan. 2004.

[10] M. H. Bakr, J. W. Bandler, K. Madsen, and J. Søndergaard, "Review of the space mapping approach to engineering optimization and modeling," *Optimiz. Eng.*, vol. 1, pp. 241–276, 2000.
[11] K.-L. Wu, Y.-J. Zhao, J. Wang, and M. K. K. Cheng, "An effective dynamic coarse model for optimization design of LTCC RF circuits with aggressive space mapping," *IEEE Trans. Microw. Theory Tech.*, vol. 52, no. 1, pp. 393–402, Jan. 2004.
[12] M. A. Ismail, D. Smith, A. Panariello, Y. Wang, and M. Yu, "EM-based design of large-scale dielectric-resonator filters and multiplexers by space mapping," *IEEE Trans. Microw. Theory Tech.*, vol. 52, no. 1, pp. 386–392, Jan. 2004.
[13] F. W. Wang, W. T. Wang, S. X. Gong, S. Zhang, and Y. Q. Zhang, "Implicit space mapping applied to the synthesis of antenna arrays," *Progr. Electromagn. Res. M*, vol. 17, pp. 283–295, 2011.
[14] S. Koziel and S. Ogurtsov, "Rapid design optimization of antenna using space mapping and response surface approximation models," *Int. J. RF Microw. Comput. Aided Eng.*, vol. 21, no. 6, pp. 611–621, Nov. 2011.
[15] S. Tu, Q. S. Cheng, J. W. Bandler, and N. K. Nikolova, "Space mapping design exploiting library antenna models," presented at the IEEE AP-S/URSI Int. Symp. Antennas Propag., Chicago, IL, Jul. 2012.
[16] Antenna Magus. ver. 3.2, Magus (Pty) Ltd., South Africa, 2011.
[17] W. Geyi, Q. Rao, S. Ali, and D. Wang, "Handset antenna design: Practice and theory," *Progr. Electromagn. Res.*, vol. 80, pp. 123–160, 2008.
[18] J. W. Bandler, Q. S. Cheng, N. K. Nikolova, and M. A. Ismail, "Implicit space mapping optimization exploiting preassigned parameters," *IEEE Trans. Microw. Theory Tech.*, vol. 52, no. 1, pp. 378–385, Jan. 2004.
[19] J. W. Bandler, S. Koziel, and K. Madsen, "Space mapping for engineering optimization," *SIAG/Optimiz. Views-and-News, Special Issue on Surrogate/Derivative-Free Optimiz.*, vol. 17, no. 1, pp. 19–26, Mar. 2006.
[20] S. Koziel, J. W. Bandler, and K. Madsen, "Towards a rigorous formulation of the space mapping techniques for engineering design," in *Proc. ISCAS*, Kobe, Japan, Jun. 2005, pp. 5605–5608.
[21] Q. S. Cheng, J. W. Bandler, and S. Koziel, "Space mapping design framework exploiting tuning elements," *IEEE Trans. Microw. Theory Tech.*, vol. 58, no. 1, pp. 136–144, Jan. 2010.
[22] M.-C. Huynh and W. Stutzman, "Ground plane effects on planar inverted-F antenna (PIFA) performance," in *Proc. Inst. Elect. Eng., Microw. Antennas Propag.*, Aug. 2003, vol. 150, no. 4, pp. 209–213.
[23] The MathWorks, MATLAB. Natick, MA, USA, Feb. 2010. [Online]. Available: http://www.mathworks.com/products/matlab/
[24] *"FEKO User's Manual,"* EM Software & Systems, Inc., USA, Sep. 2010. [Online]. Available: http://www.feko.info, suite 6.0
[25] The MathWorks Inc., Matlab Help. Natick, MA, USA, Feb. 2010, ver. 2010a.
[26] J. Ollikainen, O. Lehmus, M. Fischer, and P. Vainikainen, "Internal dual-band patch antenna for mobile phones," in *Proc. Mill. Conf. Antennas Propag.*, Davos, Switzerland, Apr. 2000, pp. 363–366.
[27] K.-L. Wong, *Planar Antennas for Wireless Communications*. Hoboken, NJ: Wiley, Dec. 2002, pp. 31–34.
[28] M. H. Bakr, J. W. Bandler, R. M. Biernacki, S. H. Chen, and K. Madsen, "A trust region aggressive space mapping algorithm for EM optimization," *IEEE Trans. Microw. Theory Tech.*, vol. 46, no. 12, pp. 2412–2425, Dec. 1998.
[29] S. Koziel, J. W. Bandler, and Q. S. Cheng, "Robust trust-region space-mapping algorithms for microwave design optimization," *IEEE Trans. Microw. Theory Tech.*, vol. 58, no. 8, pp. 2166–2174, Aug. 2010.

**Sheng Tu** (S'12) was born in Hubei, China, in 1985. He received the B.Eng. degree in electrical engineering (Hons.) from Northwestern Polytechnic University, Xi'an, China, in 2007, the M.A.Sc. degree in electrical engineering (Hons.) from Xidian University, Xi'an, China, in 2010, and is currently pursuing the Ph.D. degree in electrical engineering at McMaster University, Hamilton, ON, Canada.

In 2010, he joined the Computational Electromagnetics Research Laboratory, McMaster University, where he is currently a Research Assistant. His research interests include electromagnetic modeling and optimization as well as microwave imaging and antenna design.

**Qingsha S. Cheng** (S'00–M'05–SM'09) was born in Chongqing, China. He received the B.Eng. and M.Eng. degrees in automatic control from Chongqing University, Chongqing, China, in 1995 and 1998, respectively, and the Ph.D. degree from McMaster University, Hamilton, ON, Canada, in 2004.

In 1998, he joined the Department of Computer Science and Technology, Peking University, Beijing, China. In 2004, he joined the Simulation Optimization Systems Research Laboratory as a Postdoctoral Fellow, then as a Research Associate Academic, and later as Research Engineer. He has consulted for Bandler Corporation, Dundas, ON, Canada. He was a Sessional Lecturer and a Committee Member of Engineering I with the Faculty of Engineering, McMaster University, from 2007 to 2010. He has published more than 70 technical papers and workshop presentations. His research interests include space mapping, simulator-based tuning, surrogate modeling and design, statistical modeling and yield optimization, modeling and design of microwave and radio-frequency circuits, and computer-aided design software design technologies.

**Yifan Zhang** (S'10) received the B.Eng. degree (Hons.) in electronic and information engineering from Harbin Institute of Technology, Harbin, China, in 2008, and the Ph.D. degree in electrical and computer engineering from McMaster University, Hamilton, ON, Canada.

In 2008, he joined the Computational Electromagnetics Research Laboratory, Department of Electrical and Computer Engineering, McMaster University, where he was a Teaching/Research Assistant. During 2011, he was a Ph.D. intern with the Advanced Technology Group, BlackBerry, Waterloo, ON, Canada. He has authored and co-authored more than 15 journal and conference papers, and patents. His research interests include forward and inverse solutions in electromagnetics with applications in biomedical imaging and nondestructive testing, antenna design and measurements, and high-frequency computer-aided analysis and design.

Dr. Zhang received the "Provincial Excellent Graduate" award from the Heilongjiang Provincial Department of Education in 2008. He was also the recipient of a "Graduate Studies International Excellence" scholarship from McMaster University in 2012.

**John W. Bandler** (S'66–M'66–SM'74–F'78–LF'06) received the B.Sc (Eng.), Ph.D., and D.Sc. (Eng.) degrees from the University of London, London, U.K., in 1963, 1967, and 1976, respectively.

He joined McMaster University, Hamilton, ON, Canada, in 1969. Currently, he is a Professor Emeritus. He was President of Optimization Systems Associates Inc. (OSA), which he founded in 1983, until 1997, when OSA was acquired by Hewlett-Packard Co. He is President of Bandler Corporation, Dundas, ON, Canada, which he founded in 1997. He has published more than 480 technical papers.

Dr. Bandler is a Fellow of several societies, including the Canadian Academy of Engineering and the Royal Society of Canada (since 1987). In 2004, he received the IEEE MTT-S Microwave Application Award "For application of optimization technology, design with tolerances and yield-driven design to microwave devices, circuits and systems." In 2012, he received the IEEE Canada A.G.L. McNaughton Gold Medal, which honors "outstanding Canadian engineers recognized for their important contributions to the engineering profession." He was also honored in 2012 by a Queen Elizabeth II Diamond Jubilee Medal. In 2013, he received the IEEE MTT-S Microwave Career Award.

**Natalia K. Nikolova** (S'93–M'97–SM'05–F'11)} received the Dipl. Eng. degree in radio engineering from the Technical University of Varna, Bulgaria, in 1989, and the Ph.D. degree in electrical engineering from the University of Electro-Communications, Tokyo, Japan, in 1997.

From 1998 to 1999, she held a Postdoctoral Fellowship of the Natural Sciences and Engineering Research Council of Canada (NSERC), during which time she was initially with the Microwave and Electromagnetics Laboratory, DalTech, Dalhousie University, Halifax, NS, Canada, and, later, for a year with the Simulation Optimization Systems Research Laboratory, McMaster University, Hamilton, ON, Canada. In 1999, she joined the Department of Electrical and Computer Engineering, McMaster University, where she is currently a Professor. Her research interests include theoretical and computational electromagnetism, inverse scattering and microwave imaging, as well as methods for the computer-aided analysis and design of microwave structures and antennas.

Prof. Nikolova was the recipient of a University Faculty Award of NSERC from 2000 to 2005. Since 2008, she has held a Canada Research Chair in High-frequency Electromagnetics. Currently, she serves as a Distinguished Microwave Lecturer. She is also a member of the Applied Computational Electromagnetics Society and a correspondent of the International Union of Radio Science.